Update on the NASA Glenn Propulsion Systems Lab Ice Crystal Cloud Characterization (2015)

Judith F. Van Zante[1], Timothy J. Bencic[2], and Thomas P. Ratvasky[3]
NASA Glenn Research Center, Cleveland, OH, 44135

NASA Glenn's Propulsion Systems Lab, an altitude engine test facility, was outfitted with a spray system to generate ice crystals. The first ice crystal characterization test occurred in 2012. At PSL, turbine engines and driven rigs can experience ice crystal icing at flight altitudes, temperatures and Mach numbers. To support these tests, four ice crystal characterizations have been conducted in two different facility configurations. In addition, supercooled liquid and mixed phase clouds have also been generated. This paper will discuss the recent learning from the previous two calibrations. It will describe some of the 12-parameter calibration space, and how those parameters interact with each other, the instrumentation used to characterize the cloud and present a sample of the cloud characterization results.

Nomenclature

CDP	=	Cloud Droplet Probe, drop sizing probe, 2 – 50 um
CF	=	Concentration Factor
CIP	=	Cloud Imaging Probe, drop sizing probe, 15 – 930 um
DeltaP	=	Pwat - Pair (psid)
Escort	=	PSL's steady state data acquisition and processing system
I	=	Intensity of light from tomography measurement
IKP	=	Iso-Kinetic Probe, water content probe
iWC	=	Ice Water Content (g/m^3)
LWC	=	Liquid Water Content (g/m^3)
MVD	=	Median Volumetric Diameter (μm)
MW	=	Multi-wire, water content probe
P0	=	Tank pressure simulating altitude (psia)
P2	=	Plenum supply pressure (psia)
Pair	=	Spray nozzle atomizing air pressure (psig)
Particle	=	Ice crystal or liquid drop issued by the spraybar system.
Ps1	=	Pressure, static at Sta 1
PSD	=	Particle Size Distribution
Pwat	=	Spray nozzle water pressure (psig)
RHPL	=	Relative humidity in the plenum (%)
RP	=	Robust Probe, water content probe
Sta 1	=	Station 1 or calibration plane, just upstream of engine/rig

[1] Technical Lead: Icing, Facilities and Test Division, 21000 Brookpark Rd, MS 6-2, and AIAA Senior Member.
[2] Optical Specialist, Instrumentation and Controls Division, 21000 Brookpark Rd, MS 77-1, and AIAA Senior Member.
[3] Aerospace Engineer, Research and Technology Division, 21000 Brookpark Rd, MS 11-2, and AIAA Senior Member.

Tair = Temperature of spray atomizing air, measured at bar inlet
TPL = Total temperature measured in the plenum (F)
Ts1 = Temperature, static, at Sta 1
Twat = Temperature of spray water, measured at bar inlet
Twb = Temperature, Wet Bulb (F), subscript t for total, s for static
TWC = Total Water Content (g/m^3)
Wa = Air mass flow rate (lbm/s)
Wf = Water mass flow rate from spraybars (lbm/s)
um = micron

Subscripts for TWC
00 = Measured TWC value at the duct center from either the IKP, MW or RP
Bulk_Meas = Calculated bulk (average) TWC based upon a measured Tomography-determined concentration factors and measured TWC_{00}
Bulk_Fit = Calculated bulk (average) TWC based upon a curve fit to the Tomography-determined concentration factors
Escort_Fit = Escort curve fit calculation of measured bulk TWC
Wf = Calculated bulk (average) TWC based upon the injected water flow and air mass flow rates. Assumes cloud is uniform within full Station 1 duct.
Wf_BL = Calculated bulk (average) TWC based upon the injected water flow and air mass flow rates. Assumes a cloud boundary layer, .i.e., no cloud in outer band.

I. Introduction

NASA Glenn's Propulsion Systems Laboratory (PSL), an altitude engine research test facility, was outfitted in 2010 with a spray system for the purpose of introducing ice crystals into the face of a running turbine engine or driven rig (Ref. 1, 2 & 3). Since then, starting in 2012 four ice crystal and icing cloud characterization efforts have occurred. The third and fourth efforts were in preparation for both the 2015 Honeywell LF11 Engine Test (Ref. 4, 5 & 6), and the March 2016 Fundamental Ice Crystal Icing study, hereinafter referred to as the Fundamental Study (Ref. 7). For the Fundamental Study, glaciated, mixed-phase and supercooled liquid clouds were investigated to simulate the ice accretion sites within an engine's core flow path.

II. Facility Description

The base calibration configuration utilizes a 36-in duct, or 27:1 contraction ratio from the spraybars in the plenum, see Fig. 1 and Fig. 2a. For this case, the calibration plane, or Station 1, is about 22-ft from the spraybars, and the constant-area 36-in duct begins about 20-ft from the spraybars. Three of the four icing test have been conducted in this configuration. The other configuration calibrated thus far was for a customer's driven rig, seen in Fig. 2b. New duct-work from the 88-in bulk head was custom-built. For this configuration, the open duct calibration plane was much closer, and the aspect ratio only 11:1. A bullet nose simulating the spinner was installed for the second portion of the calibration. With the bullet nose, the contraction ratio was 22:1. Since custom designs are possible, each new configuration requires an aero-thermal and cloud characterization. The duct size range is

- Custom duct size from 24 to 84-in

Conditions simulating flight are set by pumping down the 39-ft long by 24-ft diameter tank to the desired pressure altitude, P0, then increasing the externally conditioned air pressure supplied to the plenum, P2. The adiabatic, isentropic relationship between these two defines the Mach number. Temperature, TPL, is controlled by turbo expanders. To control and stabilize relative humidity in the plenum, RHPL, steam can

be injected well upstream of the plenum so that it is fully mixed at the plenum. The water vapor content in the plenum is measured by a Spectra sensor. These four parameters set the airflow condition. Ranges are

- Pressure altitude, *P0*, from 12.7 to 2.78 psia, corresponding altitudes from 4 to 40 kft
- Mach up to 0.8, or Air Mass Flow Rate, *Wa*, from 50 to 330 lbm/s
- Inlet total temperature, *TPL*, from -50 to +50 F
- Plenum relative humidity, *RHPL*, from ambient (0.3 to 3%) to 50%.

The cloud is issued from spraybars in the plenum, shown in Fig. 3a. The nozzles are the same as in PSL's sister facility, Glenn's Icing Research Tunnel (IRT). There are 110 Standard (higher flow) and 112 Mod1 (lower flow) nozzles. Each nozzle can be individually selected to spray. PSL has one water manifold, and two air manifolds – one per nozzle set. The spray pressures are referenced to the plenum pressure, P2. To spray a mixed phase or liquid cloud, generators can be rented to heat the spraybar air and water. Typically filtered, but non-demineralized city water is used. This helps ensure nucleation sites for particle freeze-out. However, PSL can also de-ionize (DI) the water. As seen in Fig. 3b, each nozzle is surrounded by 8 ports from which cooling air can be issued. Cox & Co. Inc., who designed the system (Ref. 8), added these to help ensure the liquid water drops would freeze. Thus, the spray condition controls include:

- Nozzle set, Standards or Mod1s
- Water Pressure, *Pwat*, from 10 to 350 psid
- Air Pressure, *Pair*, from 5 to 90 psid
- Water Temperature, *Twat*, from 45 to 180 F
- Air Temperature, *Tair*, from 45 to 180 F
- Water source, from 'city' to de-ionized
- Spraybar Cooling Air Pressure, *SBCA-P*, optional, from 5 to 30 psid
- Spraybar Cooling Air Temperature, *SBCA-T*, optional, from -20 to 40 F

III. Cloud Characterization

The cloud characterizations (Ref. 9, 10) occur prior to an engine or driven rig icing test. With the above bullets, one can see that the cloud characterization parameter space is fairly large at 12 parameters. This is significantly more complex than most icing wind tunnels. For example, the IRT has 4 parameters. The first three ice crystal cloud characterizations, with some added points for supercooled liquid, focused heavily on exploring the spraybar pressures at the primary flight condition of interest to the research test. Some exploration into the other parameters revealed a non-linear relationship between many of the 12 parameters. With this, the fourth calibration explored less of the spray parameter space, and more of the airflow parameter space, e.g., the effects of altitude and temperature. The strong effect of relative humidity had already been established in the first calibration. The cloud characterization regions with respect to PSL's icing operational environment and Part 33 Appendix D (Ref. 11) are shown in Fig. 4. The separate calibration regions in Fig. 4a reflect both the desire to simulate the aircraft flight environment as presented to the face of the engine, and, per the Fundamental Study, the environment behind the fan inside the core flow path where the ice crystal icing accretion occurs.

The physics of the PSL process is such that the liquid water drops, which issue from the spraybars into an unsaturated plenum, immediately start to cool and evaporate. The amount of evaporation and freezing is a primarily function of temperature, relative humidity and altitude, as well as air mass flow rate, the amount of water mass injected, particle size distribution, spraybar temperatures, and spraybar cooling air. As the particles travel further into the contraction, they accelerate and cool/freeze even more due to the static temperature drop and accompanying static wet-bulb temperature drop, Twb_s. Despite the increase in relative humidity, the static wet-bulb temperature decreases due to the static temperature drop in the contraction. If saturation is reached, Twb_s equals static temperature. At saturation, it is speculated that some of the water vapor re-deposits onto the existing particles; preferentially on ice crystals over water

drops due to their difference in saturation vapor pressure. An effort to model this phenomenon for PSL has recently begun and is described in Ref. 12. Briefly, this code couples the thermal interaction between the air, ice and water particles. The model had pretty good success with the well-understood physical processes. There is room for improvement to model all the "knobs" PSL can turn, such as increasing Twat and Tair. This code can help predict the phase of the cloud at Station 1.

This paper will describe the results from the recent cloud characterizations. Elements discussed include:

A. Cloud Uniformity
B. Total Water Content
C. Particle Size
D. Particle Temperature and Phase

A. Cloud Uniformity

A step in characterizing the cloud is to document cloud uniformity and density. As each nozzle is individually controlled, the nozzle pattern can be tuned to meet research needs. For example, ensuring no ice accretes on the plenum or contraction walls will result in a cloud with a thick cloud-free boundary layer. Thinner cloud boundary layers are possible, if ice accretion or ice crystal deposition on the contraction walls is acceptable. Cloud tomography is a non-intrusive method that can measure the particle number density and water content uniformity of the PSL cloud. The techniques comparing a grid to a laser sheet to a tomography system were documented in Ref. 9, and are shown again in Fig. 5. With the good agreement between the three techniques, an example is shown in Fig. 6, the tomography has been the tool of choice for subsequent calibrations.

The tomography duct can be seen in Fig. 1; it is the black spool piece which sits upstream of Sta 1 or the engine fan face. The ring contains 60 lasers and 120 detectors flush-mounted in a plane. Each laser is expanded into a fan-beam so as to illuminate as many detectors as possible on the opposite side as shown for a duplicate duct in Fig. 7. Cloud tomography is conceptually similar to medical tomography; it produces the highest spatial resolution at the duct center, with increasingly lower resolution toward the walls. This system is non-intrusive and can measure ice crystal, liquid water or mixed-phase clouds.

As described in Ref. 10, the tomography procedure is to acquire a cloud-off measurement just prior to each spray as a cloud-off reference. The lasers are synchronized with the detection system with individual sources pulsed on in a circular fashion while recording the response of all the detectors. The system then operates again with the cloud on. The attenuated intensities due to cloud particles in the flow are recorded by each fiber optic coupled detector. The natural log of the ratio of the cloud on to cloud off intensity is calculated and the tomographic reconstruction is computed generating a 2-D map of the cloud. The system is typically run for 30 – 60 sec to obtain a time-averaged cloud. It can be run on demand and return initial particle number density and uniformity results within 3 to 4 seconds. Fully processed results can be available within several minutes.

The output is the intensity, I_{ij} at pixel (i, j) over the tomography plane. Thus, tomography can provide a Concentration Factor, *CF*, of the cloud in a plane upstream of Sta 1 or the engine face. The statistics of the cloud are calculated including the mean, maximum value and standard deviation. It should be noted that, due to the approximately 6-in thick cloud boundary layer and the low resolution of the tomography data at the duct perimeter various masks can be applied in processing the data. Both 30-in and 24-in diameter masks were developed. The mask does not change the intensity data inside the chosen diameter, but forces to zero the values outside. Presented here are the results of the 24-in mask, which eliminated the adverse effects of a very sparse cloud creating noise between 24 to 30-in.

Sample tomography data are shown in Fig. 8. These are from the nozzle pattern optimization effort during the Fundamental Study test. For this study, the goal was to have the cloud fully contained within the inner 24-in diameter, and uniform over central 6-in diameter. To achieve this, several nozzles at the center were turned off. The circles depicted are of diameters 36-in (the duct outer wall), 30-in (limit of 'high-confidence' tomography data), and the research targets of 24-in and 6-in. Not shown is the center 1x1-in box used to calculate an average intensity, I_{00}, which would correspond to the TWC measured by the various sensors. The PSL data acquisition system's Escort reading, E#, as well as the concentration factor, CF, are noted above the intensity data. The intensity values are normalized by I_{00}, and therefore are between 0 and 1.2. In Fig. 8a, the widest-spread cloud for the test program – high altitude, low speed, high atomizing air pressure – is shown in Fig. 8b the narrowest-cloud – low altitude, high speed, low Pair – is shown. Both of these cases were Mod1 nozzles sprays. A Standard nozzle spray is shown for the widest-spread cloud in Fig. 8c.

A 3-D visualization of the tomography profiles is shown in Fig. 9. In this representation, one can think of the flow as going from bottom to top. The perimeter of the duct has zero cloud and therefore zero intensity, that is shown as the base. The cloud is tallest/thickest near the center. Note the profile is similar to a partially developed channel flow; it is neither the initial top-hat profile, nor the fully developed parabolic shape.

Tomography has become the preferred method to measure the uniformity of the cloud whether liquid, ice crystal or mixed phase. The light extinction is driven by the particle size (specifically the projected area of the particle) and particle number density. For the first efforts, these were measured only at the duct center and assumed uniform throughout the cloud. Scatter in the cloud uniformity measurements suggests further information and processing algorithms might be needed. There is variation in the particle size distribution and number density radially, the potentially non-circular shape of the particles (i.e., ice crystals) as well as movement of the cloud at a time scale faster than required for a full scan, which is currently about 2 seconds.

B. Total Water Content

As illustrated in Ref. 4 for one engine, TWC is the more significant factor driving its power loss events. Therefore, it is important to know the TWC presented to the face of the engine or driven rig. This section first discusses measuring TWC at the center point of the Sta 1 duct. Then discusses ways to examine the average or bulk TWC across the Sta 1 plane.

Instrumentation Description

Two different types of instruments are used to characterize the cloud water content in PSL. The first type is commonly referred to as "hot-wire" water content instruments; the second type is a total water content evaporator probe. Each is shown in Fig. 9. The hot-wire probes utilize sensing elements of different shapes and sizes which exhibit different collection efficiencies with respect to particle size and phase: ice or water (Ref. 13, 14). The water content level is determined by the electrical power required to maintain the sensing elements at a constant temperature in the presence of cloud water. The hot-wire instruments used in PSL are the Science Engineering Associates (SEA) WCM-2000 Multi-Element Water Content System (also known as Multi-wire, MW) and the WCM-3000 Robust Probe, RP. The MW design features a 2-mm diameter, concave "half pipe" (TWC element) in the center of a circular shroud, which is flanked by a 2-mm diameter convex "half pipe" (0.083 LWC element) and a 0.5-mm wire (0.021 LWC element). A more complete description of the probe can be found in Ref. 15 and an analysis of the MW probe in liquid conditions in Ref. 16. The RP features a 3.8-mm diameter concave "half pipe" TWC element embedded in a heated strut (Fig. 9b). It has a ruggedized design to estimate TWC in mixed phase and glaciated conditions in wind tunnels and in flight. The MW and RP were used in the first three Calibration efforts. The RP was also used onboard the SAFIRE Falcon 20 during the High Altitude Ice Crystal-High

Ice Water Content (HAIC-HIWC) International Field Campaigns in Darwin 2014 and Cayenne 2015, as well as the Airbus flight tests in high ice water content regions (Ref. 17).

The second type of instrument was an iso-kinetic total water content evaporator probe (IKP), see Refs. 18 & 19. This type of instrument works on the principle of ingesting air and cloud particles into the probe isokinetically (no loss or gain of cloud particle mass), evaporating all hydrometeors regardless of phase, then measuring the total water vapor (background + evaporated liquid water drops and/or ice particles). The total water content of the hydrometeors is determined by subtracting the background water vapor from the total water vapor measured by the IKP. The isokinetic evaporator probe (IKP2) was used in the third and fourth PSL calibrations efforts, and is shown installed in PSL in Fig. 9c. The IKP2 was developed by SEA, with the evaporator designed and fabricated by the National Research Council Canada. The IKP is a newer technology, but still mature enough to have a body of data associated with it. In ice crystal conditions, in both tunnels and flight campaigns, the IKP2 consistently reads higher than the MW or RP (Ref. 20) due to mass loss on the hot-wire sensors. The IKP2 was the primary TWC instrument used during the HAIC-HIWC International Field Campaigns to characterize the TWC environment for Part 33 Appendix D conditions. A description of the development and performance testing of the IKP2 can be found in Ref. 20.

Data Acquisition

For a set of spray and airflow conditions, measurements of TWC are made at the center-point (0, 0) of the 36-in diameter calibration plane at Sta 1 using either the MW, RP or IKP2. These instruments were installed sequentially for center-point measurements. The process for acquiring the TWC data is the same as described for the IRT in Ref. 16. It was to 1) set the airflow conditions and acquire pre-spray baseline measurements, 2) turn the spray system ON to generate the cloud for 2-3 minutes and acquire the cloud-on TWC and tomography measurements, then 3) turn the spray system OFF to get post-spray baseline measurements. The TWC at each spray and airflow condition was then determined by averaging the TWC during cloud on, minus the cloud on/off transients.

Operational Notes for the MW

To ensure more uniform flow quality at the hot-wire sensing elements, a splitter plate is used. The leading edge of the plate is beveled and optionally heated. Without the plate, the flow at the sensor head is both angled so that the element and compensation wire can be shadowed as well as highly turbulent due its proximity to the mounting strut. The plate further protects the elements from the effects of any ice accretion or deposition on the mounting strut. The MW and splitter plate installed at Sta 1 are shown in Fig. 9a.

For the MW, the collection or *collision* efficiency analysis conducted in Ref. 21 on the sensing elements within the sensor head was applied to the data. The collision efficiency only accounts for particles that impinge on the elements, not subsequent losses due to bouncing or splashing. From this, Ref. 22 created a spreadsheet that accepts a particle size distribution and calculates the collision efficiency on each element at user specified pressure, temperature and airspeed. When applied it is noted with '_Em'. The correction is more pronounced for lower momentum (smaller, slower) particles. For these tests, the correction factor ranges from 0.94 to 0.99. Such an analysis has not yet been conducted for the wider RP without the shroud, so values presented here are as measured or raw.

The minerals in the city water tended to coat the sensing elements. It became expected that the probe would not be able to return valid data for a whole run shift. Therefore, several "health check" points are inserted throughout a run shift. That is, a condition at the beginning of the run is repeated to look for a degraded response from the heated elements. If found, then either a time-costly midcell (shutting down flow and returning the test cell to ambient pressure to enable access) is required to replace the probe with

a clean one, or trend-only data were taken, e.g. an altitude sweep. Trend-only data are excluded when determining calibration curve fits.

Sample MW Time Data

The MW is the oldest of the technologies used to characterize TWC in PSL. It has the advantage that it can indicate the phase of the cloud, which the other two sensors cannot. The ratios of the cylindrical elements, 083 and 021, to the half-pipe, TWC can indicate phase for a given particle size. Ratios closer to zero indicate glaciation, while ratios closer to one indicate liquid. Sample MW time traces are shown in Fig. 10. These traces are for given airflow and spray conditions, with only the sweep parameter changing. In Fig. 10a, the temperature decreases in time. Note how the TWC stays relatively constant, while the response of the cylindrical elements decreases. The ratios 083/TWC and 021/TWC dropped from 0.56 and 0.44 respectively at the warmest temperature to 0.23 and 0.20 at the coldest temperature. These particles are "medium" sized, with MVD in the 40 to 70 um range. The effects of relative humidity are shown in Fig. 10b. Both the individual water contents as well as the 083/TWC and 021/TWC ratios are plotted. The total wet bulb temperature, Twb_t, is also indicated on the graph. One can see the phase of the cloud is governed by whether Twb_t is greater or less than freezing, and, in this case, it is driven by RHPL. This cloud has smaller particles, around MVD = 20 um.

Sample IKP2 Time Data

A typical time-history from the IKP2 results is shown in Fig. 11. Spray ON is show with the dashed line shifting from 0 to 1. The pre-spray baseline water vapor measurements made with the IKP2 and the background water vapor system were reset to match the PSL facility water vapor measurement (PSL_MMR_S1) made at Sta 1. For the IKP2, the averaging time typically started about 30 seconds after Spray On to account for the time lag in the background water vapor rise. The rise in background water vapor was associated with the evaporation of spray water occurring. The amount of rise depended on the RHPL value, static temperature at Station 1, and the spray settings. The time lag in the rise of background was due to the transport time from the background humidity inlet to the background water vapor sensor (LICOR LI-840A) and was a function of tubing size, length and flow rate. The background humidity inlet used for this test is shown in Fig. 12. It was a reverse-flow inlet with a cone deflector to reduce ice or water contaminating the background water vapor readings. It was mounted at the base of the calibration duct at Station 1 with the air inlet about 2.5-in from the wall. It should be noted that during the fourth calibration for the Fundamental Study, a water vapor sensor inlet was traversed across the duct, and a radial distribution was observed. However, for the high-altitude, low-temperature conditions, the bias in the IKP2 TWC measurement caused by the offset in background humidity is expected to be less than 5% of the reading.

Calculated Bulk TWC from Water Flow

A crucial step is to develop a basis function for TWC. The basis function shall be a means to calculate TWC based upon facility measurands (measured quantities). For the IRT,

$$\text{LWC\_IRT} = \text{fn (Nozzle Type, Pair, DeltaP, Airspeed)} \quad (1)$$

The basis for the PSL cloud water content characterization is more complicated. In addition to the spray nozzle settings (Nozzle Type, # Nozzles, Pair, DeltaP) each of the airflow settings (pressure, Mach, temperature, and relative humidity) help define the total water content of the cloud at Sta 1. It seems that the calculated air mass flow rate, Wa, which encompasses the airflow parameters except RHPL, is a useful parameter. The TWC basis formulation to date, valid for a range of pressures and Mach numbers, but at fixed temperature and plenum relative humidity, is

$$\text{TWC\_PSL} = \text{fn (Wf, Wa, Ts1, Ps1)} \quad (2)$$

where Ts1 and Ps1 are the static temperature and static pressure at Sta 1. The injected water flow rate, Wf, is a simple calculation. It is a fair assumption for the Configuration 1 tests to date that all the water injected arrives at Sta 1 in one phase or another; no water mass is deposited on the tunnel walls.

$$Wf = \#Noz * Cfn * \sqrt{(DeltaP)} \quad (3)$$

Where #Noz is the number of nozzles spraying and Cfn is the calibrated flow coefficient for the Mod1 or Standard nozzles.

One can make a calculation of bulk or average TWC based soley upon these ratios of the water injection to air mass flow rate. Such a calculation would assume the cloud is uniformly distributed thoughout the 36-in duct duct at Sta1. This calculation is,

$$TWC\_Wf = C * Wf * Ps1 / (Wa * Ts1) \quad (4)$$

Where C is a constant that includes the density of water at 0ºC and conversion factors. An in-house code predicted the Sta 1 parameters from the customer-supplied fan face static conditions assuming isentropic conditions.

If one assumes there is no cloud in a boundary layer of thickness *delta* in the *R* radius duct, the equation transitions to

$$TWC\_Wf\_BL = C * Wf * Ps1 / (Wa * ((R-delta)/R))^2 Ts1) \quad (5)$$

These equations are based upon facility measurands, or isentropic, adiabatic calculations from measured quantities. The effects of evaporation and re-condensation are ignored. Ultimately, during the LF11 Engine test, this TWC_Wf_BL calculation was used to set the spray condition.

Measured Bulk TWC from Sensor and Tomography

A different approach to calculating the bulk, or average TWC over the Sta 1 cross-section plane comes from combining the TWC and tomography measurements described in Section III A. This process takes the cloud spatial intensity data over the tomography plane, I_{ij}, it's center average, I_{00}, and the central TWC, or TWC_{00}, as measured by the IKP2, RP or MW probes. As they cover the same region, the central intensity, I_{00}, is related to the measured TWC_{00}. Their ratio is applied to all intensities, I_{ij}, times the area they cover, A_{ij}. The values are summed, then divided by the total area covered,

$$TWC\_Bulk\_Meas = \sum (I_{ij} * (TWC_{00}/I_{00}) * A_{ij}) / \sum A_{ij} \quad (6)$$

Tomography data was acquired on most sprays, but not all. Therefore, a fit to the tomography concentration factor, *CF*, data as a function of Pair and TWC_Wf was developed for both Mod1 and Standard nozzles. The curve fits have significant scatter in them, probably due to assumptions made regarding the radial uniformity of the cloud in particle size and number density. Even with the scatter, the CF curve fits provide a way to estimate the bulk TWC from measured data even without a corresponding tomography measurement. Using the curve-fit CF instead of the measured CF is denoted with TWC_Bulk_Fit.

Data from this process is shown in Fig. 14. At the anchor point airflow conditions, the range of Mod1 spray conditions in nozzle number, the measured bulk TWC values (Eq. 6), are plotted for each of the sensors against TWC_Wf. As expected, the IKP2 returned significantly higher TWCs than the RP or MW for the same conditions. It was known that the scatter in the IKP and RP data was due to different particle sizes. The larger the particle MVD, the higher the measured TWC at the center point. This can be seen

more clearly in Fig. 15, where the same IKP and RP data sets are plotted by groups of MVD. This MVD effect did help illustrate the CFD analyses of PSL from Refs. 30 & 23, which predict the larger drops are concentrated in the center of the duct at Sta 1. In the plenum, the low-momentum larger drops are driven to the center as they enter the contraction, then they stay there as their inertia increases. On the other hand, the smaller particles are more uniformly dispersed throughout the duct at Sta 1.

To prepare for the LF11 test, simple, linear trendlines were fit to the data, ignoring the MVD effect for now. These are indicated in Fig. 14. Note that in this paper, the results of the final IKP data and tomography CFs are presented; preliminary IKP data and tomography CFs were used to prepare for the LF11 Engine calibration. The shift between initial and final data is within 1%, well within measurement error. The following simple curve fits were programed into the Escort system:

$$\text{TWC\_Escort\_fit} = m_p * (\text{TWC\_Wf}) + b \tag{7}$$

Where the slope, m_p, is unique to each sensor as seen in Fig. 14, and the intercept, b, is set to zero.

A comparison of the two independent Bulk TWC calculations can be illustrative, and is shown in Fig. 16. Here the Escort curve fit of the Measured Bulk TWC from tomography and IKP2 and MW sensors, TWC_Escort_fit is plotted versus the water flow injected with boundary layer calculation, TWC_Wf_BL. It is encouraging that the bulk TWC measured from IKP2 and tomography is within 5% of the bulk TWC calculated from Water Flow with boundary layer.

Particle Phase Calculation

It should be noted that the default assumption from WCM-2000 (for the MW and RP) is that the elements are impinged by 100% liquid water. Per the SEA WCM-2000 User's Manual (Ref. 15), the calculation applied only accounts for heating water then phase-changing it to vapor and is

$$LWC = \frac{K * P_{sense,wet}}{\left[c_{liq}\left(T_{evap} - T_{amb}\right) + L_{evap}\right] \cdot TAS \cdot L_{sense} \cdot W_{sense}} \tag{8}$$

Ref. 15 also provided the chart showing the Phase Change Energy Requirements, duplicated in Fig. 17. The PSL M300 data acquisition system has been programmed to calculate the above, and a calculation that also includes the Heating Ice and Heat of Fusion terms:

$$iWC = \frac{K * P_{sense,wet}}{\left[c_{ice}\left(T_0 - T_{amb}\right) + L_{fus} + c_{liq}\left(T_{evap} - T_{amb}\right) + L_{evap}\right] \cdot TAS \cdot L_{sense} \cdot W_{sense}} \tag{9}$$

Thus, in PSL, two calculations are performed: the original SEA half-pipe TWC calculation which assumes a 100% liquid water environment, and a new calculation which assumes the elements are impacted by 100% ice crystals and is notated iWC. The ratio iWC/TWC has been pretty steady around 0.88 for a variety of airflow conditions.

In Fig. 18, the ratios of IKP/RP and IKP/MW_Em are shown for the same airflow and spray conditions. For the RP and MW, the ratios are given for both the standard TWC (100% liquid water) in Fig. 18a, and iWC (100% ice crystal) in Fig. 18b. Note particles greater than 100 um are not glaciated, so the corresponding iWC value was removed. For comparison, Ref. 17 stated the efficiency factor of the RP used for the flight campaigns was 0.4, which translates to 2.5 for the IKP2/RP ratio shown here. Based on preliminary results from the HAIC-HIWC Darwin flight campaign, the IKP2/RP ratio ranged from 1.6 - 2.4. The range in these values is likely due to the ice particle size range and ice habit structure.

C. Particle Size

The most difficult measurement to accurately obtain with confidence in PSL at this time is particle size. Previous studies have been conducted to understand the effects of MVD inside an engine, see Ref. 2 and 4, indicating that particle size as a secondary effect on accretion. The current instrumentation used in PSL includes the Cloud Droplet Probe, CDP, for sizes 2 to 50 um, and Cloud Imaging Probe - Grey Scale, CIP-GS, for sizes 15 to 960 um. Both probes are made by Droplet Measurement Technologies, Inc. and are shown in Fig. 19. These probes work well characterizing the spectrum of liquid particles. Sample results are shown in Fig. 20. For a liquid water case that required both probes, the particle size distribution, PSD, and cumulative volume are shown. In Fig. 20c, d, a temperature effects case is shown. The airflow and spray conditions are constant, except for the tunnel air and spray bar temperatures. For the "warm" case, Ts1 = 12 F and Tair = Twat = 180 F, for the "cold" case, Ts1 = -20 F and Tair = Twat = 45 F. One can see a slight shift in the PSD. The calculated MVD was 17.7 um for the warm case and 19.0 for the cold case.

Concerns with these sizing probes for ice crystals in PSL became apparent, however. While the MVDs returned were credible, based upon experience with these nozzles in the IRT, the number densities and therefore LWC were not. While the lead author only uses particle sizing probes for sizing, and not to measure TWC, experience has taught that the number density should monitored for indication of coincidence error – that is, the violation of the assumption that only one particle is present in the sample volume at a time. It is also noted that an opaque particle will not allow refracted light through to the sensor. Therefore, only the diffracted light component is measured. With this, the CDP is expected to slightly under measure ice crystal particle sizes (Ref. 24). The CIP is expected to be immune to the difficulties associated with the CDP, as it measures the number of diodes shadowed, subject to the grey-scale thresholds chosen.

With all the concerns, the CDP and CIP data are still well ordered, and curve fits to the data were obtained. Fig. 21 shows the measured MVD data with their curve fits for both the Mod1 and Standard nozzles, as well as the 'goodness of fit' data. These curve fits were given to be programmed in Escort.

With the realization of difficulties described above, additional techniques to measure particle size were introduced in 2015. During both the Fundamental Study piggyback (2015) and actual test (2016), Artium's Phase Doppler Interferometer (PDI) and High Speed Imager (HSI) were installed. As can be seen in in Fig. 22, they were both installed non-intrusively at the duct exit. For the fourth calibration, the HSI measurement location could reach 18-in to the center of the duct. Data were taken at both center and off-center. Details and probe outputs from the first test are described in Ref. 25. While data from the second, more conclusive test were not processed in time for this report, sample HSI images are shown in Fig. 23. PDI and HSI data from these entries will be published in a later report.

D. Particle Temperature and Phase

The temperature and phase of the particles contained within the cloud is of high interest to researchers in the icing community. Two different methods have been investigated starting in 2005 with non-contact methods to determine whether the bulk average cloud contains liquid, ice or mixed-phase particles as well as determining the average temperature using Raman and fluorescence spectroscopy.

The Raman spectroscopic technique has long been used in the study of water and its bonded structure in the liquid phase for temperatures above and below 0°C as well as in its ice phase (Refs. 26, 27, 28). The use of Raman scattering to measure the temperature of droplets was first attempted at the GRC Icing Research Tunnel in 2005 with some success in an environment less challenging than PSL. An initial feasibility bench top calibration was performed on deionized water on a thermoelectrically controlled hot/cold plate using a commercially available Raman probe and existing argon ion laser and spectrograph. The measurement of spectra for a stationary droplet at different temperatures was relatively straight

forward; experimental data is shown in Fig. 24. The project's second phase was to use the same probe in the IRT to measure droplet temperatures at the spray nozzles and in the test section to determine the rate at which the droplets cool after being introduced in to the tunnel flow. Good data were obtained at the spray bar location where the spray densities where highest, but limitations were identified in the test section with a sparse cloud and too small of an optical probe volume. These inhibited the acquisition of any meaningful data. With that, it was uncertain whether the high speed (Mach 0.5), high number density flows of PSL would create quantifiable results.

A more extensive study using the Raman technique for cloud measurement was started in 2013 with the establishment of ice crystals in the PSL facility. It was hoped that this technique would provide the needed information regarding phase detection and particle temperature. These parameters have been measured or calculated from information acquired using Raman Lidar techniques for atmospheric cloud studies (Ref. 29). An environmental chamber was used to create the thermal conditions of PSL from +30° to -30°C. The spectra were measured as liquid water cooled to approximately -20°C. At this temperature, observations revealed ice was present, internal to the droplet, so acquisition was stopped as to not to mix the pure liquid and pure solid phases with the mixed partial phase condition. Next, the temperature was lowered to -30°C to fully freeze the particle before slowly warming the chamber and acquiring the Raman signal to the freezing point. The optical fiber coupled setup used a 180° back-scatter configuration because of limited optical access in the chamber. The spectra for the liquid and ice states are shown in Fig. 25; the values are normalized to the isosbestic point located at 646-nm for the 532-nm laser excitation as well as the shift in the ice spectra to shorter wavelengths. The shaded Area1 and Area2 are the integrated regions used to generate the calibration values in Fig. 26. The areas widths were chosen by optimizing linearity and sensitivity by varying the integrated wavelength regions. The data show that for an area ratio less than 2.0 the droplets are liquid and greater than 2.0 the water is in the ice phase. The area ratios have also been implemented using two sharp cutoff band-pass filters approximating the integrated area of the spectral regions and measured using a photo-multiplier tube (PMT) or photon counter per channel. The two signals are measured and divided providing a real-time assessment of the phase and temperature of the water particles.

Several attempts have been made to measure the phase and temperature of cloud particles in the PSL duct as well as measurements internal to an engine to determine surface water or ice. The sparse cloud and high speed flow, along with fiber-coupled laser excitation and detection lead to extremely low light levels. The optical setup utilized a 532-nm, 5-watt CW laser fiber coupled into the test cell, Raman shifted light is fiber coupled to the detection system. These initial tests have been limited to using a spectrometer to detect the signal because the very low signal does not always distinguish itself against the high background light levels observed as the characteristic Raman water signature. Higher sensitivity detectors and bulk filtering of short and long areas will be used when confidence is obtained that the water spectrum is correct.

The measurement of the bulk average cloud phase and temperature has been more elusive due to long integration times and high noise levels in the measured signal. During the fourth cloud calibration, Raman spectral measurements were acquired for several sprays: a fully super-cooled liquid cloud and a fully glaciated cloud as shown in Fig. 27. The signals have been highly filtered to yield the characteristic Raman water shape to determine the phase of the particles. Extracting the temperature is a greater challenge as it is highly dependent on the amount of filtering done to the acquired signal. The broadening of these signals is due to the use of much larger fibers in a bundle to capture more light as well as the signal filtering Spray E345 qualitatively shows some liquid content by the clear peak near 640-nm besides the ice peak near 630-nm. Sprays E303 and E348 show the possibility of liquid by the appearance of a flat area near 640-nm whereas E349 and E356 clearly shows a trough in this region indicating little to no liquid water. The optimization of the collection optics and detection system continues in an attempt to

make these types of measurements routine not only for the cloud measurement but also for internal engine surface measurements.

IV. Conclusions

This paper discusses the instrumentation and sample results that characterize the ice crystal, liquid and mixed-phase clouds in NASA Glenn's Propulsion Systems Lab to date. This is a new and unique facility, and several challenges to characterizing the cloud have been identified. It has been realized that the calibration parameter space is fairly large at 12 parameters. Cloud characterization efforts need to focus airflow parameters in addition to spray parameters, as there are apparently complex interactions between the parameters. These interactions are generally what drives evaporation in the plenum and re-condensation of the vapor as the cloud accelerates and chills toward the calibration plane at Sta 1. Furthermore, radial variations in total water content, particle size distribution and relative humidity have been identified.

Advanced optical diagnostics, such as the cloud tomography system have significantly enhanced the ability to characterize the cloud. This non-intrusive, on demand, near-real time assessment of the cloud provides a light extinction intensity map. This plane of data can be used in conjunction with center-point measured TWC values to create a measured bulk TWC. A variety of sensors has been used to measure TWC: an IKP2, MW and RP. A bulk TWC can be calculated from measureable facility parameters including the water injection rate and air mass flow rate and optionally a cloud boundary layer thickness. The cloud is assumed to be uniformly distributed in the plane, and the effects of evaporation are ignored. In comparing the two bulk TWC calculation methods, unexpectedly good agreement was shown between the tomography + IKP bulk values and the water flow with a boundary layer bulk values.

Particle size measurements have primarily been made with instrumentation common to the NASA IRT, but variations in number density and ice particle refraction/diffraction have been challenging. Other measurement technologies such as a Phase Doppler Interferometer and High Speed Imager were used in recent tests and show promise for characterizing the particle size distribution.

Some success can also be reported with an effort to measure particle phase (ice or water) and temperature in PSL. The Raman spectroscopy concept was proven on a benchtop in clean, static conditions. After some effort, it was successfully modified to be able to measure bulk temperature and phase with particles moving at Mach 0.5. Future efforts will be made to make this measurement even more robust.

Acknowledgments

Thanks to the sponsors, NASA's Aeronautics and Evaluation Test Capability, AETC, and Advanced Air Transport Technology, AATT, projects under the Advanced Air Vehicles Program. It takes insightful, strong leaders to plan, and a village to successfully execute a test in PSL. Many thanks to engine icing research leads Ashlie Flegel and Michael Oliver for their dedicated work to bring the calibrations and engine tests to fruition; test conductors Kyle Zimmerle, Queito Thomas, Tom Griffin and Patrick Rachow, for their steady leadership; Mechanical Engineers Dennis Dicki and Jack Kowalewski, Electrical Engineers, Bryan Rosine, Barry Piendl and Paul Lizanich, Data Engineers Jon Borman, Pam Poljak, Ike Eichorn and Logan Micham were all essential in their engineering prowess to achieve success, and to the folks who make things happen, the tunnel operators/technicians: Wes Alderman, John Brodkowski, Jack Colon, Danny Erbacher, Derick Espenschied, Heather Graves, Don Gonzales, Kurt Hall, Jason Jacko, Jeff Luptak, Jim Mazor, Sherri Mohn, Jeff Paulin, Jim Sexton, Kent Smith, Eric Stevens, Joe Switala, Mike Thomas, Ken Trsek, John Wargo, Adam Wasylyshyn, and Jeff Wick. Chris Lynch was able to visually document the clouds and accretions. Researchers Tadas Bartkus, Pete Struk, Jen-Ching Tsao provided valuable insights and discussion. Amy Fagan supported the advanced optical instrumentation. Finally, it was a pleasure working with the good folks from Honeywell who supported the LF01 and LF11 Engine tests.

FIGURES

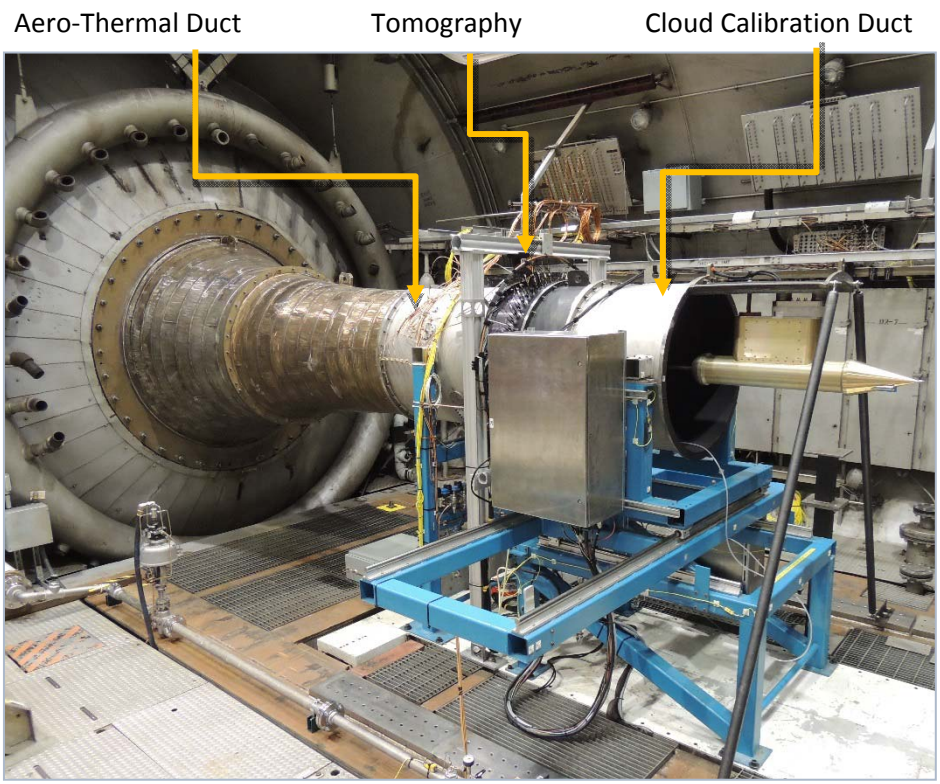

Figure 1. PSL base calibration configuration. The bulkhead and constant area ducts are indicated: Aero-Thermal duct measuring pressure, temperature and specific water vapor; Tomography and Raman Duct; Cloud calibration duct measuring water content and particle size. The Station 1 plane is at the axial center of the calibration duct.

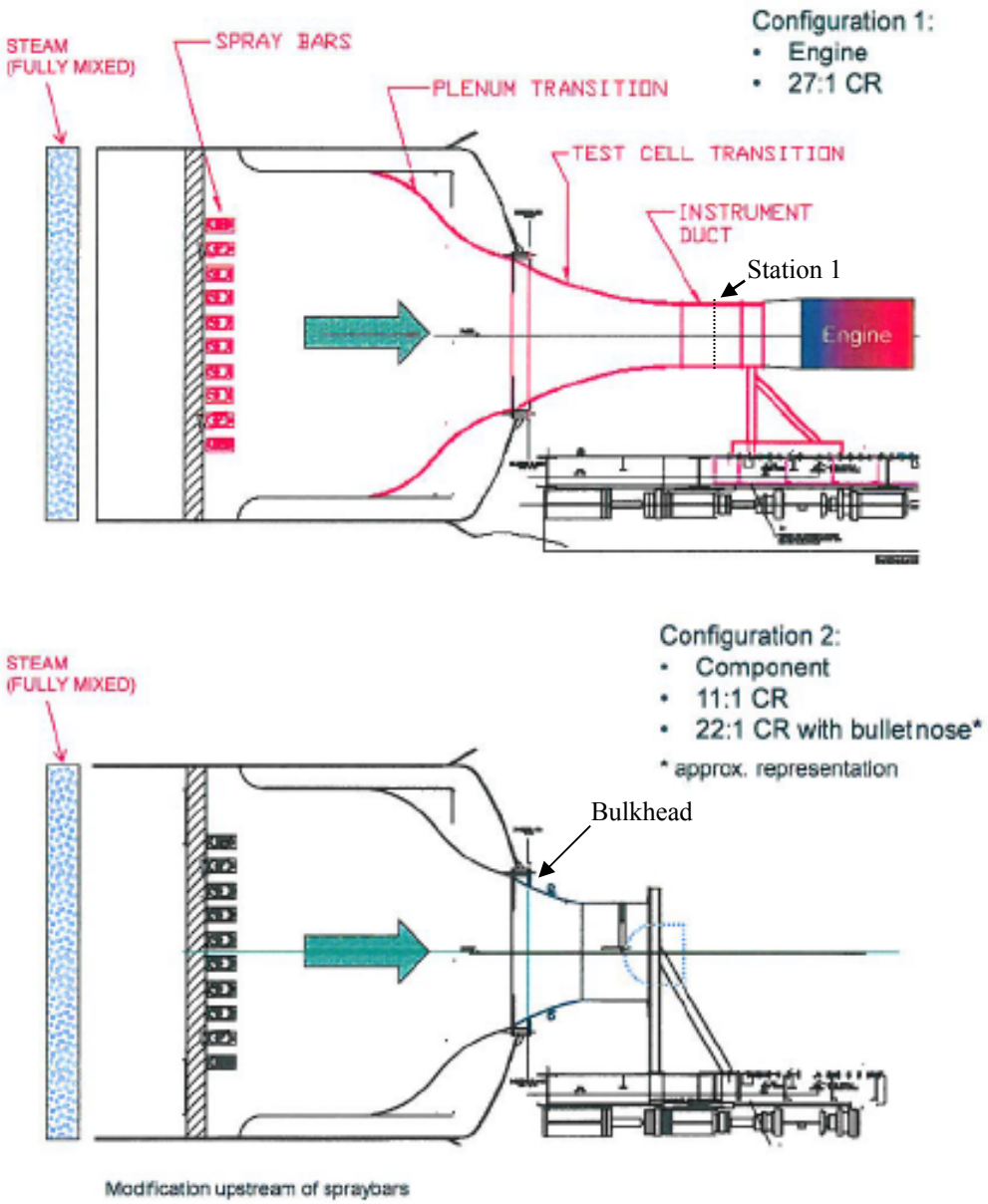

Figure 2. PSL Configuration Schematics: (a) PSL base configuration with 36-in duct and engine, (b) Calibration configuration for customer driven rig test; the bullet nose depicted above is different than the actual design. The three contraction ratios (CR) are noted.

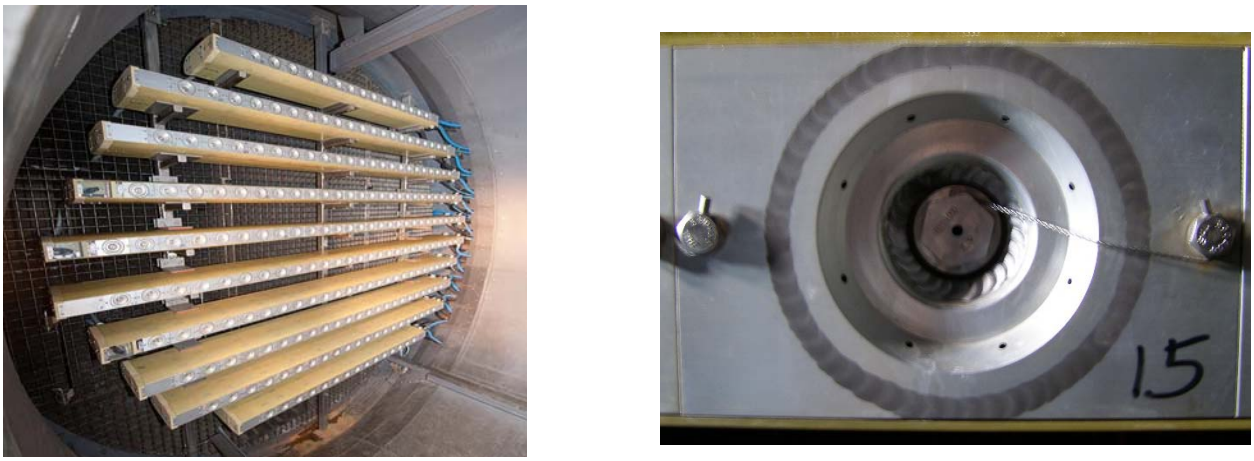

Figure 3. Spraybar setup in PSL Plenum: (a) overview, (b) close-up of nozzle exit and cooling air ports.

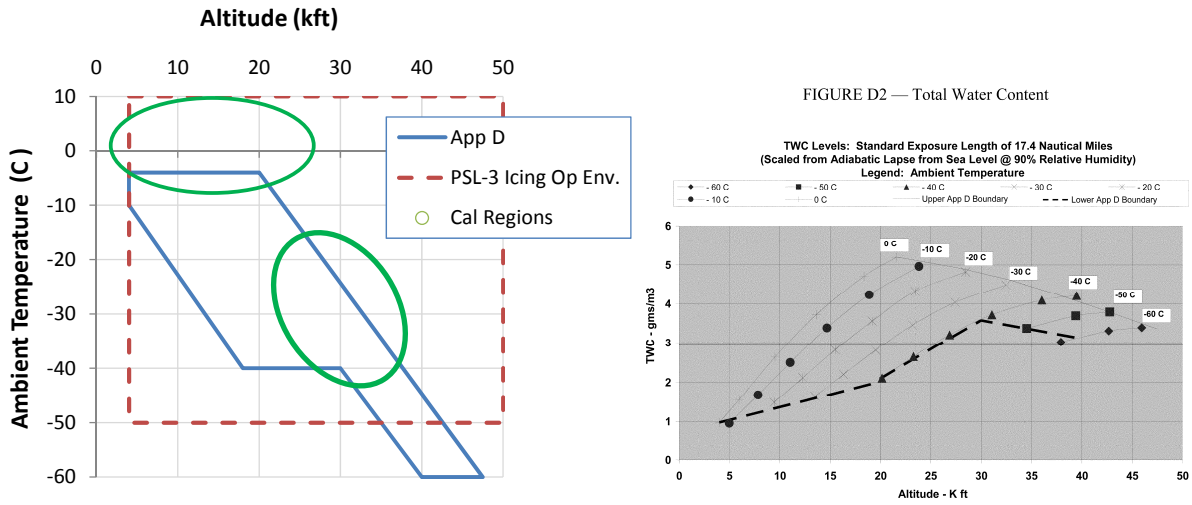

Figure 4. Cloud characterization regions to date with respect to Appendix D and PSL Icing Operating Envelop, (a) is based upon Ref. 11 Figure D1, and (b) Figure D2.

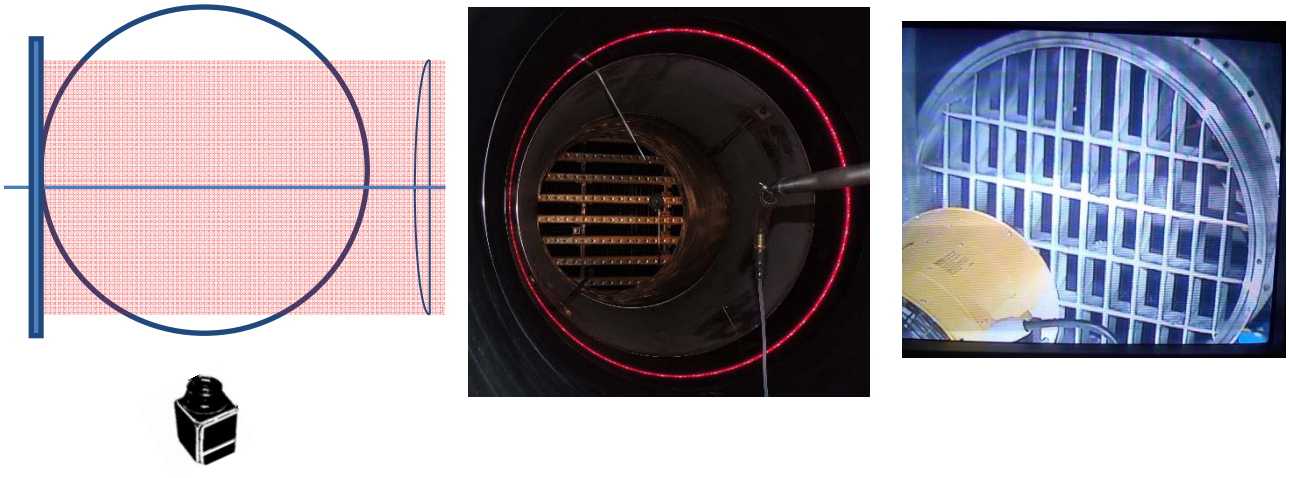

Figure 5. Cloud uniformity diagnostics, (a) laser sheet, (b) tomography duct, (c) grid.

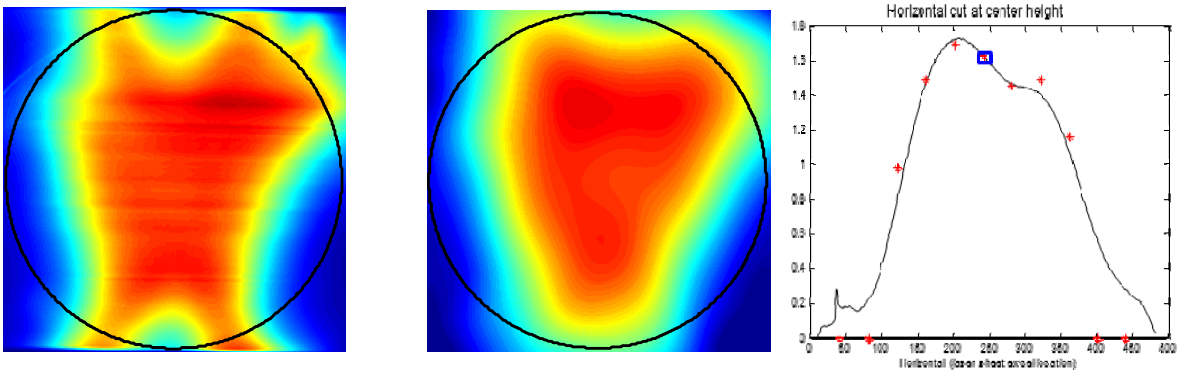

Figure 6. Cloud Uniformity results for (a) laser sheet, (b) tomography duct, (c) grid.

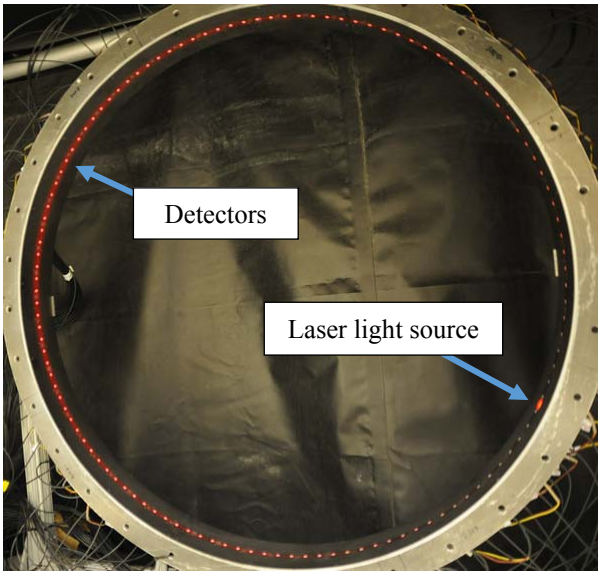

Figure 7: Tomography ring showing detectors illuminated by a single red light source. The configuration used in PSL utilizes 60 sources and 120 detectors.

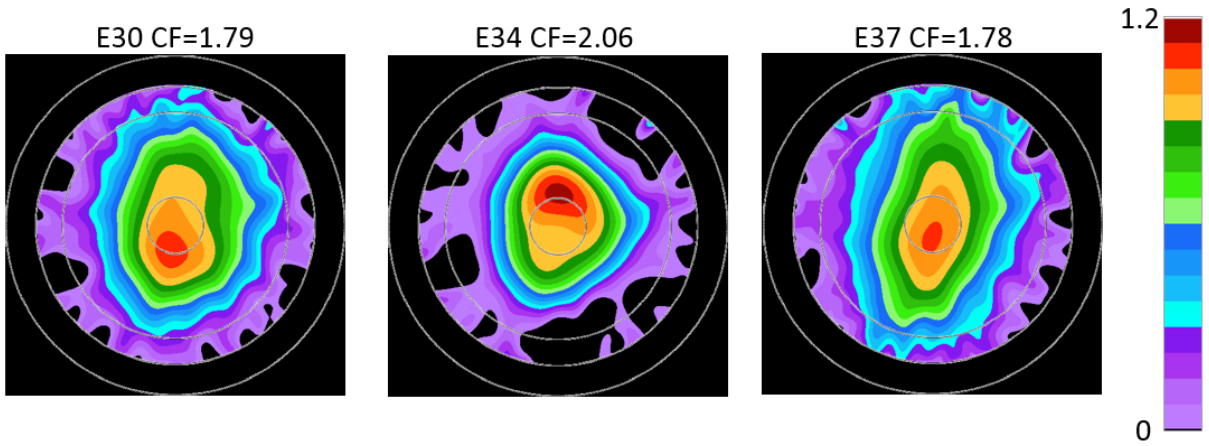

Figure 8. Sample tomography results from the Fundamental Study nozzle optimization. Circles depict diameters of 36-in (the duct outer wall), 30-in (limit of 'valid' tomography data), 24-in and 6-in (per researcher request). The Escort reading, E#, as well as the concentratin factor, CF, are noted at top. The light intensity scale from 0 and 1.2 where the intensity is normalized by the center 1-in square I_{00}. In (a), the widest spread cloud for the test matrix was expected, in (b) the narrowest cloud was expected. In (c) a Standard nozzle pattern is shown.

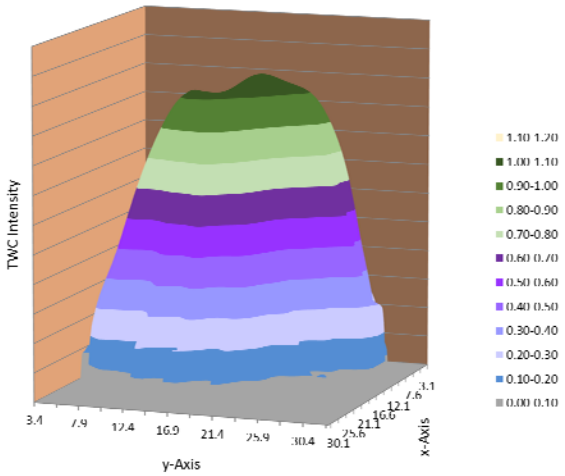

Figure 9. Tomography profile in 3-D. The horizontal axes, with zero TWC, is the central 30-in diameter circle. This example comes a Mod1 spray for engine flight conditions.

Figure 10. TWC sensors: (a) Multi-wire installed in PSL, (b) Robust Probe and (c) IKP2.

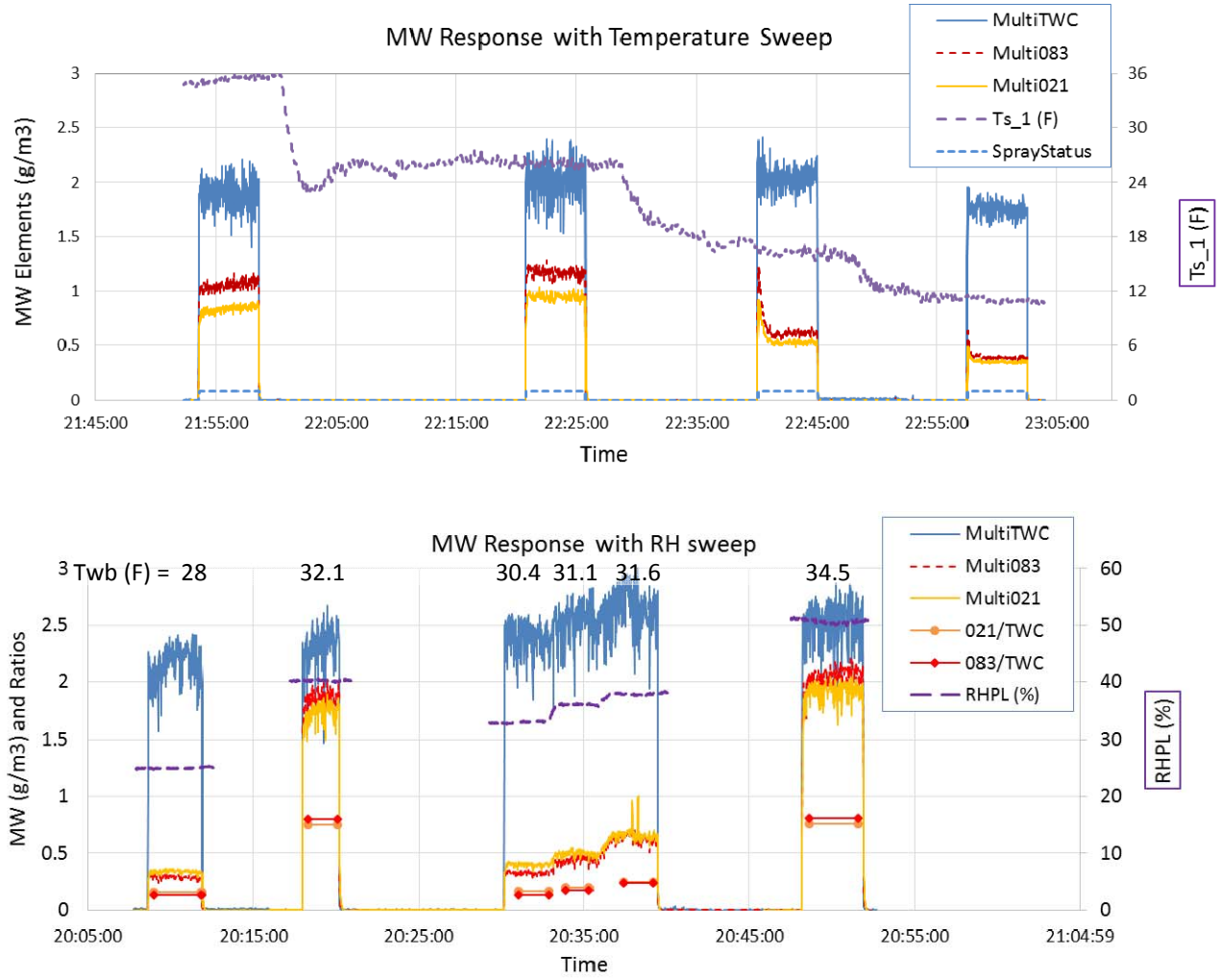

Figure 11. Sample Multi-wire responses indicating phase for sweeps in (a) temperature, (b) relative humidity. In (a) Spray On is also indicated when SprayStatus changes from 0 to 1. In (b), The ratios of 083/TWC and 021/TWC, which can indicate phase as well as particle size, are also plotted on the left axis

(max value = 1.0). The change in Twb is also noted on the chart. The RHPL values shown come from the Escort data system, which is only gathers data around Spray On.

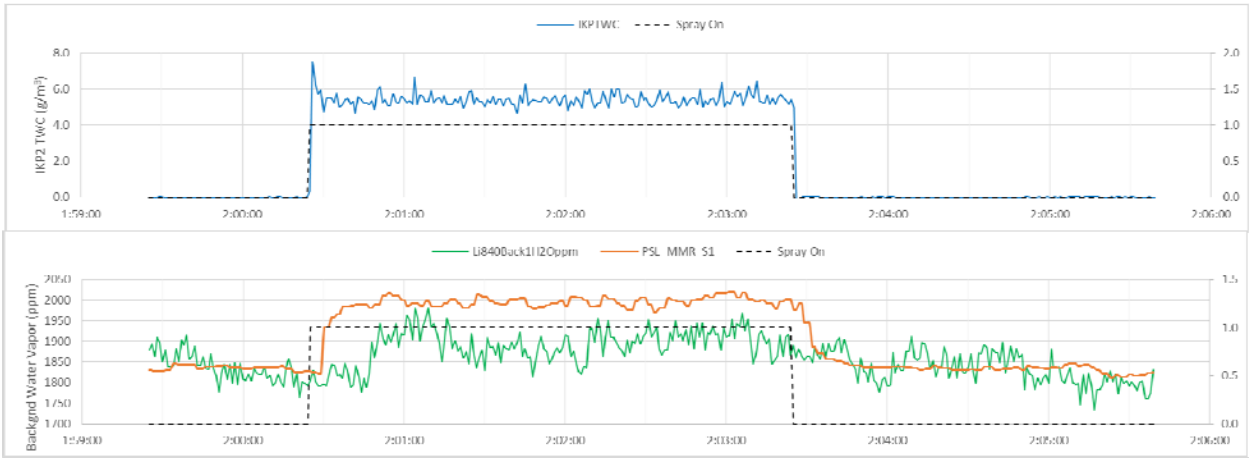

Figure 12. Typical IKP TWC and background water vapor time history.

Figure 13. Reverse Flow Background Humidity Inlet.

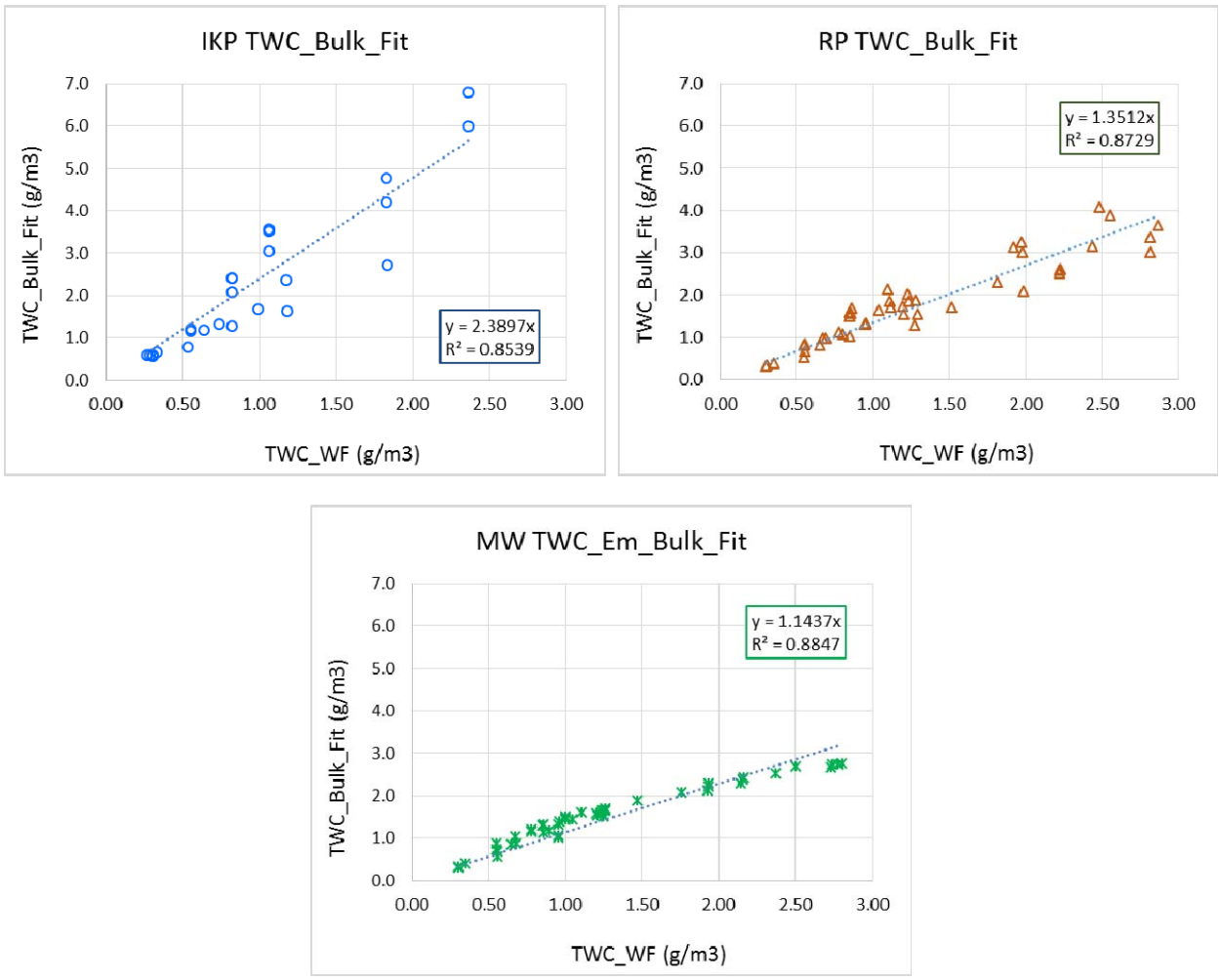

Figure 14. Bulk TWC data at a given airflow condition for Mod1 nozzles (half or full nozzle patterns) with various sensors: (a) IKP2, (b) Robust Probe, (c) Multi-Wire corrected for collision efficiency.

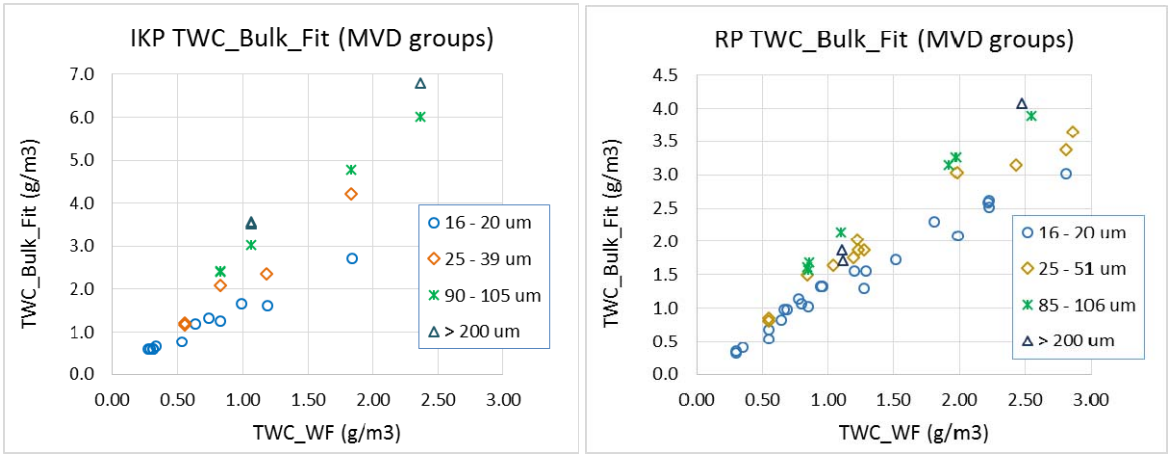

Figure 15. Measured IKP and RP Bulk TWC data plotted by MVD groups. Same data set as Fig 9.

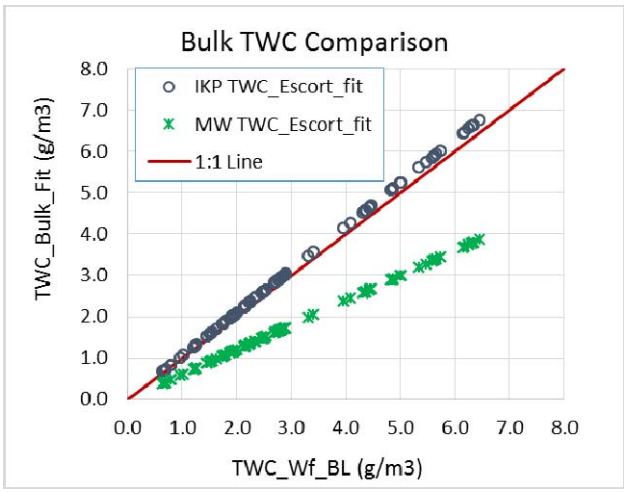

Figure 16. Comparison of Calculated vs Measured Bulk TWCs in Escort.

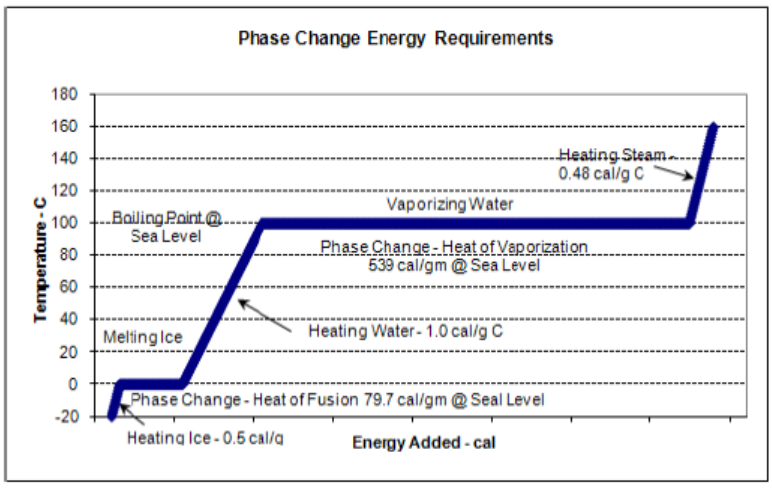

Figure 17. Energy Requirements chart from Ref. 15 illustrating requirements to change phase of water.

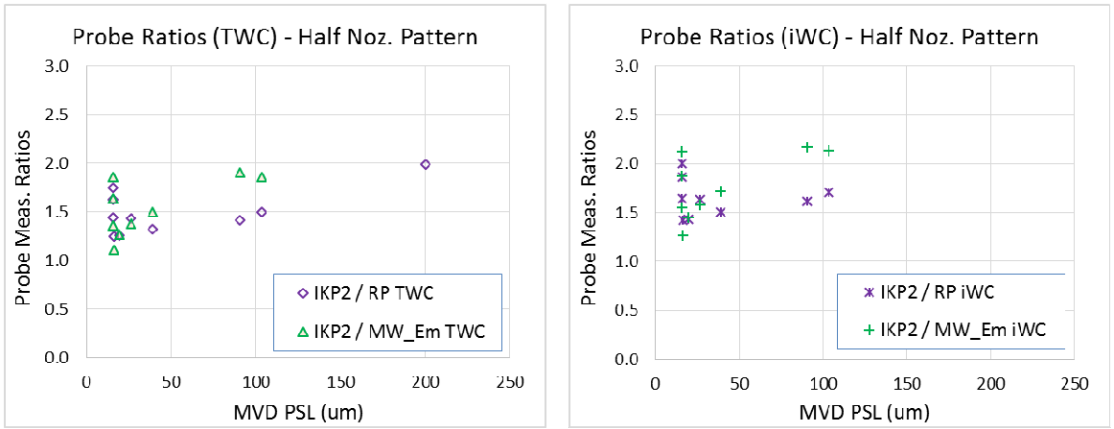

Figure 18. Measured TWC probe ratios for the Half Mod1 Nozzle Pattern (every other turned on): IKP2/RP and IKP2/MW_Em. In (a) the RP and MW values are the standard TWC calculation which assumes a 100% liquid water environment. In (b), the RP and MW values are iWC, which assume a 100% ice crystal environment.

Figure 19. PSL particle sizing instruments installed at calibration plane. (a) CDP with spray on as viewed by Spraybar camera, (b) CIP.

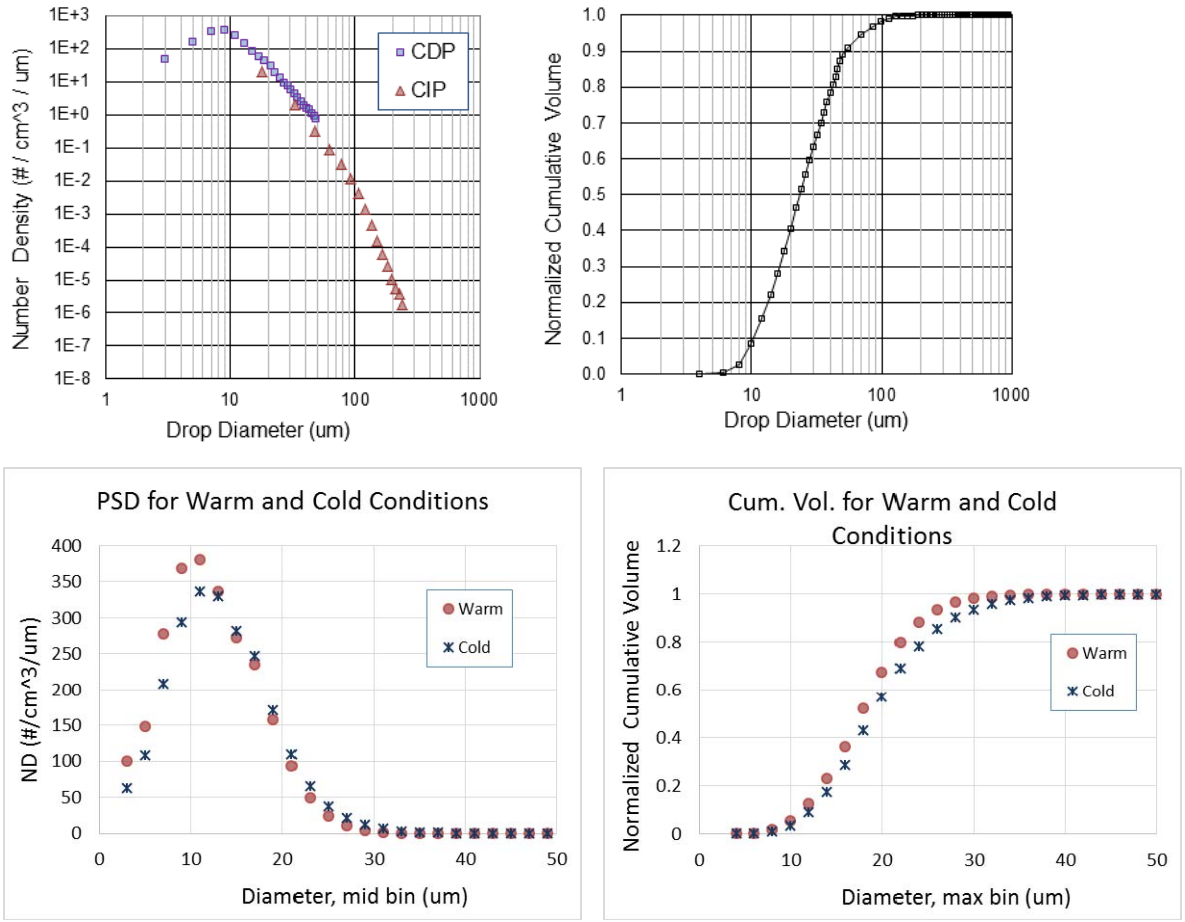

Figure 20. Sample particle size distributions (a) PSD and (b) cumulative volume in supercooled liquid water conditions, and showing temperature effects with all else being equal in (c) PSD and (d) cumulative volume.

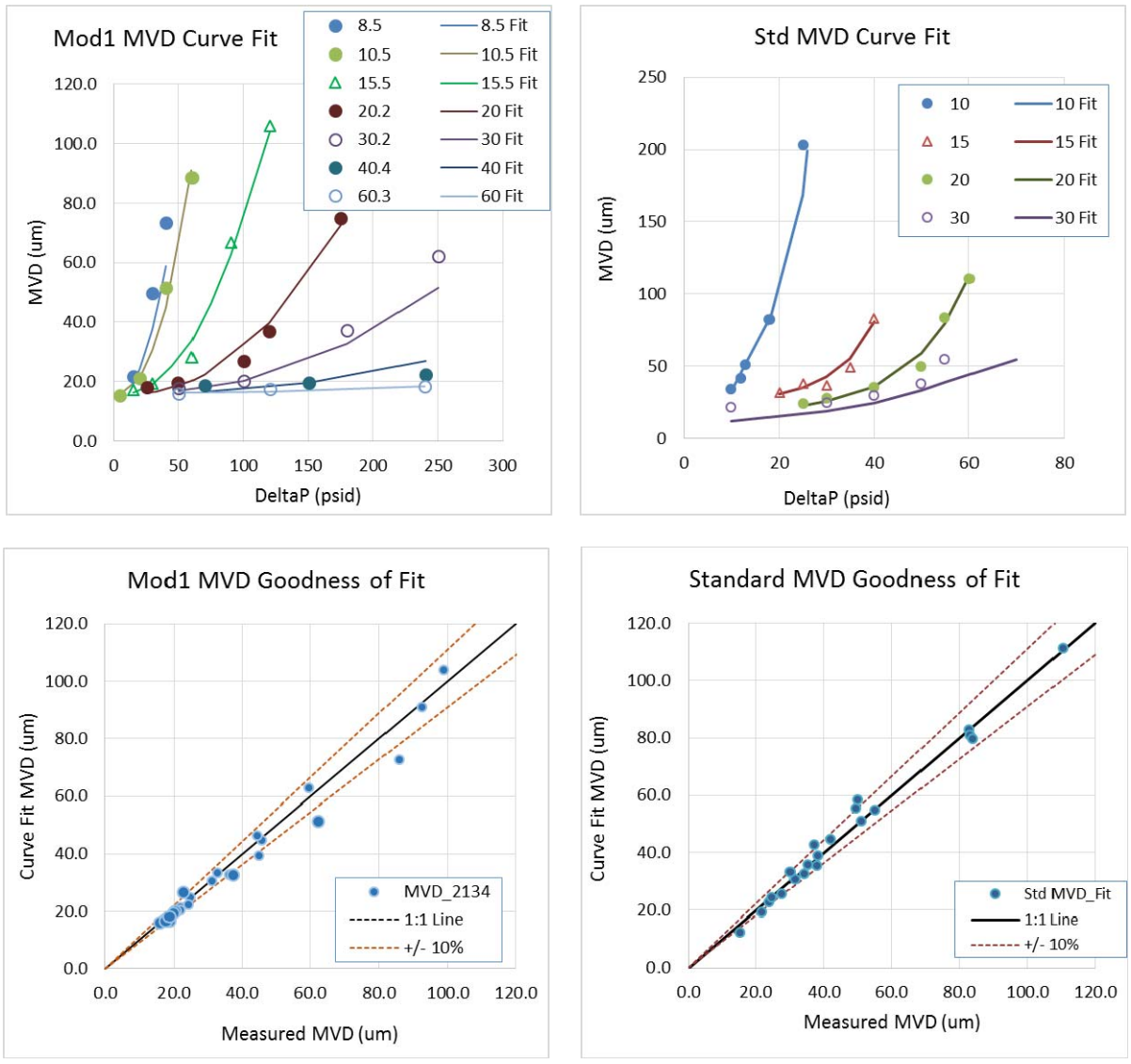

Figure 21. MVD Curve Fits. Ice crystal curve fits as a function of Pair and Delta P for (a) Mod1 Nozzles and (b) Standard nozzles; goodness of fit for (c) Mod1 nozzles and (d) Standard Nozzles.

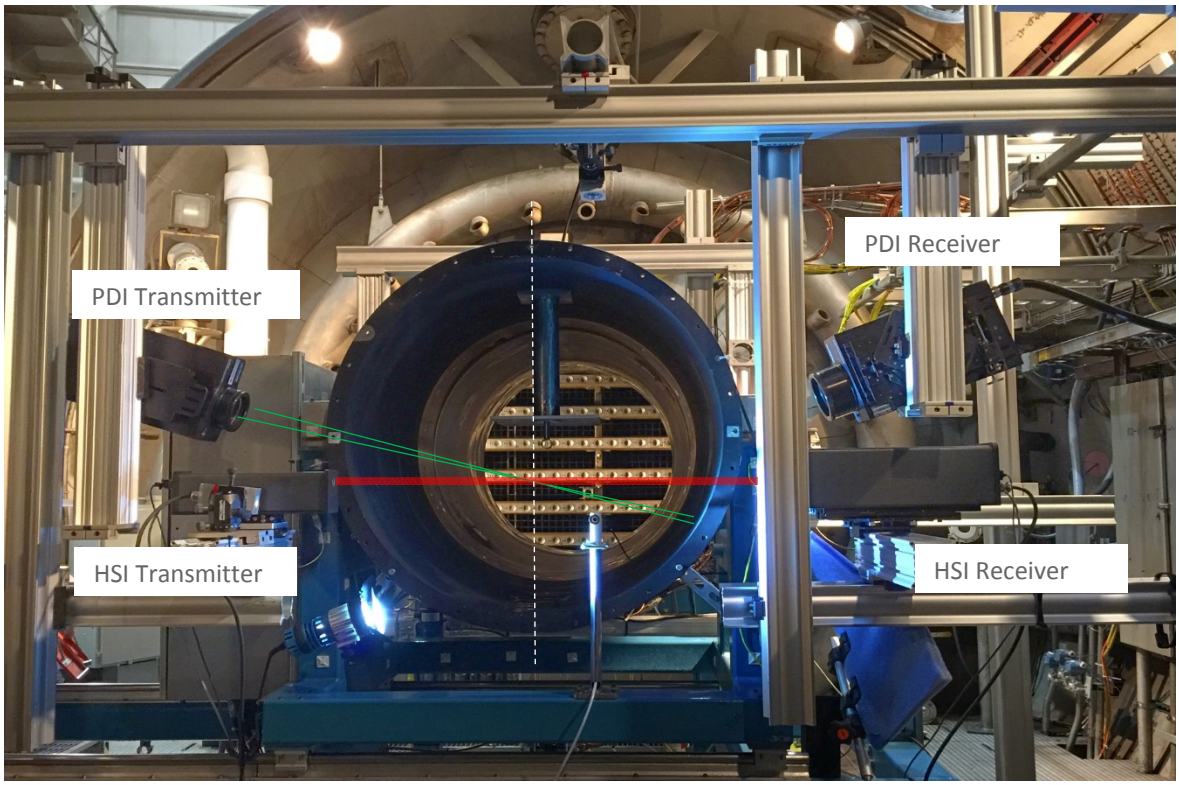

Figure 22. Artium particle sizing instrumentation, Phase Doppler Interferometer, and High Speed Imaging, as installed in PSL.

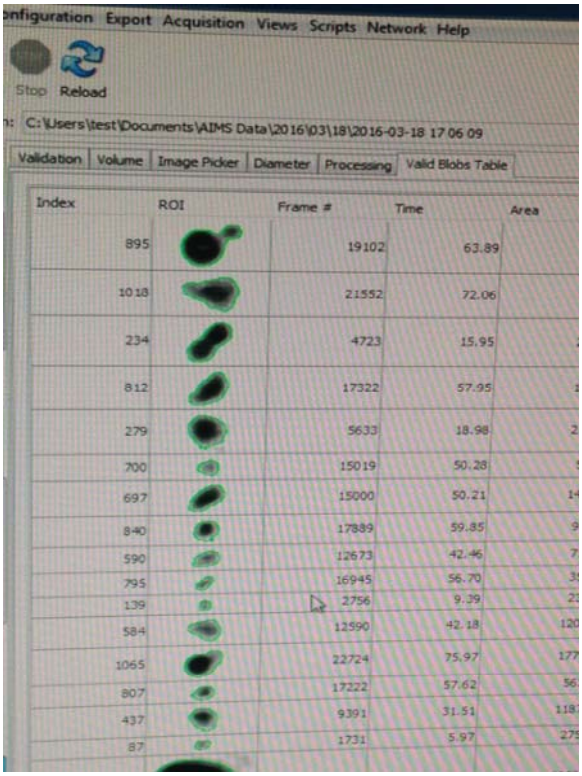

Figure 23. Sample output from HSI.

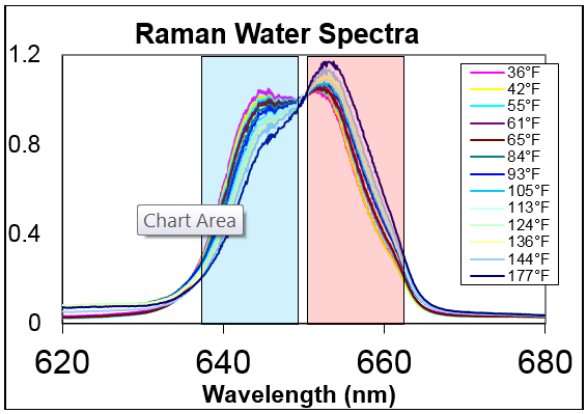

Figure 24. Raman spectra of deionized water measured in the GRC bench-top experiment on a cold plate showing the shaded areas used to generate a ratio that produces the water temperature.

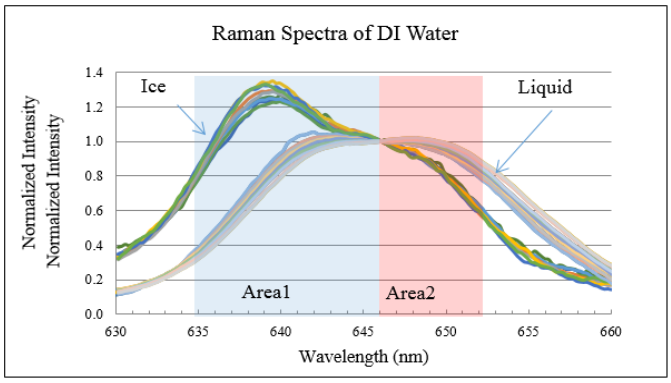

Figure 25. Plot of the Raman signal measured in the environmental chamber for both liquid and ice. The shaded areas are used to calculate an area ratio for the temperature calibration in Fig. 24.

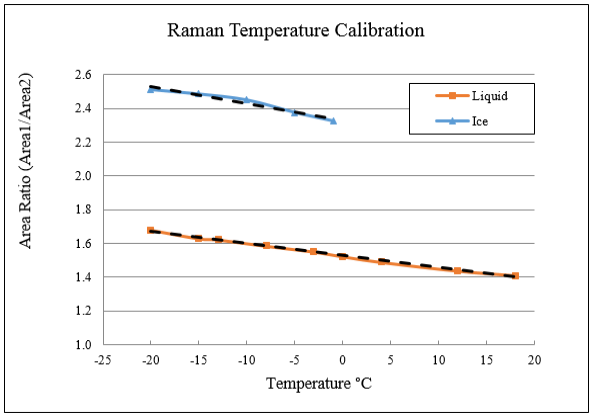

Figure 26. Plot of the Raman temperature calibration using the Areas of figure 2 on each side of the isosbestic point to determine the Area Ratio.

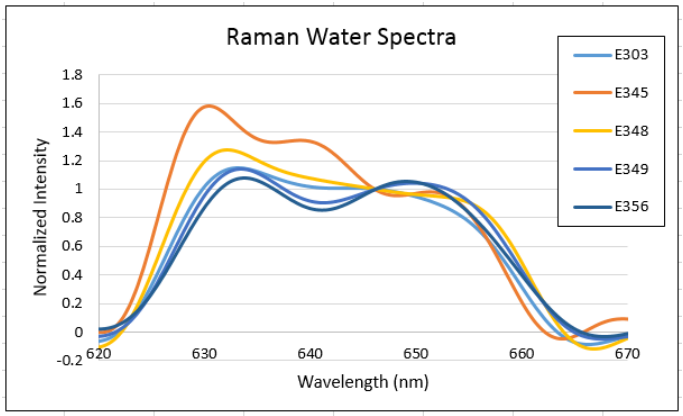

Figure 27. Raman spectral measurements of the cloud particles as they exit the duct. The appearance of the shifted peak at 630-nm is an indication of ice while the area near 640-nm indicates the presence of liquid water. Signal broadening is due to larger fiber bundle used to gather more light in this configuration.

References

1. Griffin, T.A., Lizanich, P., and Dicki, D.J., "PSL Icing Facility Upgrade Overview," *6th AIAA Atmospheric and Space Environments Conference*, Atlanta, GA, June 16-20, 2014, AIAA 2014-2896.

2. Oliver, M. J. "Validation Ice Crystal Icing Engine Test in the Propulsion Systems Laboratory at NASA Glenn Research Center," *6th AIAA Atmospheric and Space Environments Conference*, Atlanta, GA, June 16-20, 2014, AIAA-2014-2898.

3. Goodwin, R.V., Dischinger, D.G., "Turbofan Ice Crystal Rollback Investigation and Preparations Leading to Inaugural Ice Crystal Engine Test at NASA PSL-3 Facility," *6th AIAA Atmospheric and Space Environments Conference*, Atlanta, GA, June 16-20, 2014, AIAA-2014-2895.

4. Flegel, A.B., Oliver, M.J., "Preliminary Results from a Heavily Instrumented Engine Ice Crystal Icing Test in a Ground Based Altitude Test Facility," submitted to 2016 AIAA Aviation. *8th AIAA Atmospheric and Space Environments Conference*, Washington, D.C, June 13-17, 2016, (submitted for publication).

5. Goodwin, R.V., Fuleki, D., "Turbofan Ice Crystal Rollback Investigation and Preparations Leading to the Second, Heavily Instrumented, Ice Crystal Engine Test at NASA PSL-3 test Facility," submitted to 2016 AIAA Aviation. *8th AIAA Atmospheric and Space Environments Conference*, Washington, D.C, June 13-17, 2016, AIAA 2016 (submitted for publication).

6. Walker, D.J., "Determination of engine recovery after an ice accretion rollback, engine performance deterioration and health monitoring using minimal instrumentation during icing testing at NASA Glenn PSL3," *8th AIAA Atmospheric and Space Environments Conference*, Washington, D.C, June 13-17, 2016 (submitted for publication).

7. Struk, Peter M., Tsao, Jen-Ching, and Bartkus, Tadas, P., "Plans and Preliminary Results of Fundamental Studies of Ice Crystal Icing Physics in the NASA Propulsion Systems Laboratory," *8th AIAA Atmospheric and Space Environments Conference*, 13-17 June, 2016, Washington D.C., AIAA (submitted for publication).

8. Cox & Company, Inc. (Shamara, P.), "*Technology Demonstration Icing Test Report for NASA Propulsion Systems Laboratory (PSL),*" Document D-10864, Rev 2, Apr 2010.

9. Van Zante, J. F., and Rosine, B. M. "NASA Glenn Propulsion Systems Lab: 2012 Inaugural Ice Crystal Cloud Calibration," *6th AIAA Atmospheric and Space Environments Conference*, Atlanta, GA, June 16-20, 2014, AIAA 2014-2897.

10. Bencic, T.J., Fagan, A.F., Van Zante, J.F., Kirkegaard, J.P., Rohler, D.P., Maniyedath, A., and Izen, S.H., "Advanced Optical Diagnostics for Ice Crystal Cloud Measurements in the NASA Glenn Propulsion Systems Laboratory," *5th AIAA Atmospheric and Space Environments Conference*, AIAA 2013-2678, June 2013.

11. Federal Aviation Administration, Title 14 CFR Parts 25 and 33 [Docket No. FAA–2010–0636; Amendment Nos. 25–140 and 33–34], *Airplane and Engine Certification Requirements in Supercooled Large Drop, Mixed Phase, and Ice Crystal Icing Conditions*, effective: January 5, 2015, https://www.federalregister.gov/articles/2014/11/04/2014-25789/airplane-and-engine-certification-requirements-in-supercooled-large-drop-mixed-phase-and-ice-crystal

12. Bartkus, Tadas, P., Tsao, Jen-Ching, Struk, Peter M, Van Zante, Judith F., "Numerical Analysis of Mixed-Phase Icing Cloud Simulations in the NASA Propulsion Systems Laboratory," *8th AIAA Atmospheric and Space Environments Conference*, 13-17 June, 2016, Washington D.C., AIAA (submitted for publication).

13. Lilie, L., Emery, E., Strapp, J.W., Emery, J., "A Multiwire Hot-Wire Device for Measurement of Icing Severity, Total Water Content, Liquid Water Content, and Drop Diameter," *43rd AIAA Aerospace Sciences Meeting and Exhibit*, 10-13 January 2015, Reno, Nevada, AIAA-2005-859

14. Van Zante, Judy, Addy, Gene, and Ide, Bob, "*PSL/Cox Technology Demonstration II*", internal NASA Memo, Feb, 2011.

15. Science Engineering Associates, "WCM-2000 User Guide", http://www.scieng.com/ , accessed 2016.

16. Steen Laura E., Ide, Robert F., and Van Zante, Judith F., "An Assessment of the Icing Blade and the SEA Multi-Element Sensor for Liquid Water Content Calibration of the NASA GRC Icing Research Tunnel," *8th AIAA Atmospheric and Space Environments Conference*, 13-17 June, 2016, Washington D.C., AIAA (submitted for publication).

17. Grandin, A., Merle, J-M, Weber, M., Strapp, J.W., Protat, A., King, P., "AIRBUS Flight Tests In High Ice Water Content Regions," *6th AIAA Atmospheric and Space Environments Conference*, 16-20 June, 2014, Atlanta, GA, AIAA 2014-2753

18. Davison, C.R., Ratvasky, T.P., and Lilie, L.E., "Naturally Aspirating Isokinetic Total Water Content Probe: Wind Tunnel Test Results and Design Modifications," *SAE 2011 International Conference on Aircraft and Engine Icing and Ground Deicing*, 13-17 June 2011, Chicago, Illinois, SAE 2011-38-0036.

19. Davison, C., Strapp, J.W., Lilie, L.E., Ratvasky, T.P, and Dumont, C., "Isokinetic TWC Evaporator Probe: Calculations and Systemic Error Analysis," *8th AIAA Atmospheric and Space Environments Conference,* 13 - 17 June 2016**,** Washington, D.C., AIAA (submitted for publication)

20. Strapp, J.W., Lilie, L.E., Ratvasky, T.P., Davison, C., Dumont, C., "Isokinetic TWC Evaporator Probe: Development of the IKP2 and Performance Testing for the HAIC-HIWC Darwin 2104 and Cayenne 2015 Field Campaigns," *8th AIAA Atmospheric and Space Environments Conference*, 13-17 June, 2016, Washington D.C., AIAA (submitted for publication)

21. Rigby, D.L., Struk, P.M., and Bidwell, C., "Simulation of fluid flow and collection efficiency for an SEA multi-element probe," *6th AIAA Atmospheric and Space Environments Conference*, AIAA 2014-2752, Atlanta, 2014. doi: 10.2514/6.2014-2752.

22. Struk, P.M., NASA Glenn Research Center, personal communication.

23. Bidwell, C. and Rigby, D., "Ice Particle Analysis of the Honeywell ALF502 Engine Booster," SAE Technical Paper 2015-01-2131, 2015, doi:10.4271/2015-01-2131.

24. Bachalo, William, private communication, March 2016.

25. Bachalo, William, “Mixed-Phase Ice Crystal and Droplet Characterization”, NASA Contract# NNX15CC04P, SBIR Phase III Final Report, Aug. 2015

26. Durickovic, I, et. al, Water-ice phase transition probed by Raman spectroscopy, J. Raman Spectroscopy, Vol. 42, Issue 6, pgs. 1408-1412, 2011

27. Hare, D.E., Sorensen, C.M., Raman spectroscopic study of bulk water supercooled to -33°C, J. Chem Phys. 93, No. 1, 1990

28. Walrafen, G.E., Hokmabadi, M.S., Yang, W.H., Raman isosbestic points from water, J. Chem. Phys. Vol 85, No. 12, 1986

29. Whiteman, D.N., Melfi, S.H., Cloud Liquid Water and Particle Size Detection using a Raman Lidar, Proc. Ninth ARM Science Team Meeting, San Antonio, TX March 22-26, 1999

30. A. M. Kinney, Inc., Cox & Company, PEDCO, A-P-T Research, “PSL Icing Project – Icing System Final Design Report – 90% submittal”, 2.0 Icing System Analysis, Feb 26, 2010.